Uniaxial stress-driven coupled grain boundary motion in hexagonal close-packed metals: A molecular dynamics study

Hongxiang Zong,[a,b] Xiangdong Ding,[b,*] Turab Lookman,[a,*] Ju Li[b,c] and Jun Sun[b]

[a]*Theoretical Division, Los Alamos National Laboratory, Los Alamos, NM 87545, USA*
[b]*State Key Laboratory for Mechanical Behavior of Materials, Xi'an Jiaotong University,
Xi'an 710049, People's Republic of China*
[c]*Department of Nuclear Science and Engineering & Department of Materials Science and Engineering,
Massachusetts Institute of Technology, Cambridge, MA 02139, USA*

Abstract—Stress-driven grain boundary (GB) migration has been evident as a dominant mechanism accounting for plastic deformation in crystalline solids. Using molecular dynamics (MD) simulations on a Ti bicrystal model, we show that a uniaxial stress-driven coupling is associated with the recently observed 90° GB reorientation in shock simulations and nanopillar compression measurements. This is not consistent with the theory of shear-induced coupled GB migration. In situ atomic configuration analysis reveals that this GB motion is accompanied by the glide of two sets of parallel dislocation arrays, and the uniaxial stress-driven coupling is explained through a composite action of symmetrically distributed dislocations and deformation twins. In addition, the coupling factor is calculated from MD simulations over a wide range of temperatures. We find that the coupled motion can be thermally damped (i.e., not thermally activated), probably due to the absence of the collective action of interface dislocations. This uniaxial coupled mechanism is believed to apply to other hexagonal close-packed metals.
© 2014 Acta Materialia Inc. Published by Elsevier Ltd. All rights reserved.

Keywords: Grain boundary motion; Interface dislocations; Deformation twinning; Molecular dynamics; Titanium

1. Introduction

The strength and ductility of materials are inherently governed by their microstructure. In crystalline metals, for example, the mechanical properties are often associated with the way that dislocations interact with grain boundaries (GBs). Classically, one would expect an increase in the yield stress for small grain sizes (possessing a higher density of grain boundaries) to follow the Hall–Petch relation, in which the strength scales with the reciprocal square root of grain size [1–3]. However, as the structural scale reduces from the micrometer to the nanometer range, GB-mediated plasticity mechanisms (such as atomic shuffling, GB sliding and GB rotation [4–7]) are believed to be enhanced due to increasing GB density and suppression of dislocation activation [8,9]. Therefore, an improved understanding of the GB-based plastic deformation process is critical for the design of desirable mechanical properties.

Among possible GB-based mechanisms, shear-driven coupled GB migration has been observed to be dominant in both experiments [10–12] and molecular dynamics (MD) simulations [5,13,14]. Although most studies have focused

on face-centered cubic (fcc) (e.g. Cu [5], Ni [12], Al [15]) and hexagonal close-packed (hcp) metals (e.g. Mg [11,16]), it is believed that such coupling is responsible for stress-driven GB motion and stress-induced grain growth in nanocrystalline materials in general. During the coupled GB motion, the boundary produces shear deformation of the lattice and causes relative translation of the grains parallel to the GB plane. The coupling effect can be characterized by a coupling factor $\beta = V_{//}/V_n$, where $V_{//}$ is the in-plane translation and V_n is the normal boundary displacement. It has been shown that such coupling depends not only on the GB crystallography (for perfect coupling, $\beta = 2 \tan(\theta/2)$, where θ is the tilt angle and $\theta < 90°$) but also on the GB velocity, temperature, etc. [5,17]. For instance, the shear-driven coupling factor can decrease with increasing temperatures, and the GB migration mechanism changes to rigid sliding (coupling disappears) at high temperatures [17].

Atomic computer simulation studies on fcc bicrystals reveal that such shear-driven coupled GB migration can be considered as a dislocation line mediated plastic deformation process. In symmetrical low-angle GBs (LAGBs), the mechanism of shear-driven coupled GB migration is known to be the collective glide of parallel edge dislocations, forming the GB, in response to the Peach–Koehler forces imposed by the shear stress τ. The shear deformation of

---

*Corresponding authors; e-mail addresses: dinxd@mail.xjtu.edu.cn; txl@lanl.gov

the region traversed by the dislocations leads to a coupled lateral translation of the grains [17]. In high-angle GBs (HAGBs), however, the pure dislocation model is no longer applicable. Nevertheless, it was found that shear-driven coupling still exists at low temperatures. Theoretical studies have indicated that the coupled GB motion in HAGBs can be interpreted as a composite action of mobile interfacial dislocations and localized atomic shuffling [18]. However, due to the limited number of slip systems available for dislocation glide in hcp metals, the evolution of dislocation-mediated plasticity is slow and deformation twinning (DT) has been thought to occur as a major rate-limiting factor. Therefore, the DT assisted GB migration is prevalent in hcp metals [19]. For example, Zhang et al. noted that deformation twinning dominates the $[10\bar{1}0]$ tilt GB motion in magnesium, whereas the coupling is in agreement with the theory of shear-driven coupled GB motion [20].

Recently, a new mechanism for GB motion, where the lattice orientation across the GB differs by 90°, was reported in simulations of hcp-Ti single crystals undergoing shock compression normal to its prismatic plane [21]. This boundary migration process is modeled as a transformation-like lattice reorientation accompanied by a collective action of dislocations and deformation twins. This is in contrast to the 90° GB in fcc metals (such as {112} boundaries), where shock compression cannot induce the GB normal motion, only the emission of Shockley partial dislocations [22,23], and no lattice reorientation occurs. Experimentally, a similar boundary motion mechanism was observed in submicron single-crystal Mg undergoing compression along the same crystallographic orientation ($[0001]$) [24]. Although the reorientation mechanism is similar to shear-driven coupled GB motion in HAGBs, it is not clear how it relates to the conventional mechanism of shear-coupled grain boundary motion. Therefore, of fundamental interest is (1) to understand how this lattice reorientation mediated GB migration couples to external stress, and to (2) investigate how the coupling of this mode compares (in properties such as temperature dependence) to the shear-driven GB migration.

In this study we investigate the grain boundary motion in hcp metals using MD methods. Our simulations on $[10\bar{1}0]$ oriented Ti bicrystals, where the lattice orientation across the GB differs by 90°, show that the GB motion is coupled to a uniaxial stress, and not to the shear as proposed by the theory of shear-driven coupled GB migration. We describe in Section 2 the simulation methodology used to study the uniaxial stress-driven GB motion. In Sections 3 and 4, we determine the atomic mechanisms of GB motion and the underlying reason for the uniaxial stress-driven coupling effect. In addition, the geometrical factors, such as GB inclination and GB misorientation (non-90° GB) that are associated with the GB motion are also discussed. Similar to the shear-driven coupling factor, we define a new parameter to describe the uniaxial stress-driven coupling, and analyze the influence of temperature on the coupling parameter, further demonstrating a distinct coupling characteristic from the shear-driven GB motion. Finally, the main results and conclusions are summarized in Sections 5.

2. Simulation methods

The atomic interactions of the pure Ti model system studied are described by the interatomic potential developed by Zope and Mishin [25]. The potential accurately reproduces physical properties that are important in the context of this study. In particular, they predict accurate values of the elastic constants and stacking fault energies, as well as twin boundary energies.

A GB was created by constructing two separate crystals with desired crystallographic orientations and joining them along a plane normal to the y-direction, as shown in Fig. 1. Periodic boundary conditions were applied in the x- and z-directions parallel to the GB plane. In the y-direction, the grains were terminated at the free surfaces. Each grain has an approximate cubic shape. Two 1.5 nm thick slabs at the top and bottom of the box (Fig. 1a) contain atoms with relative positions frozen to those of the perfect lattice. These are used to impose a compression or tensile stress on the GB. Typical samples contain 1.74 million atoms with dimensions $L_x = 23.6$ nm, $L_y = 37.5$ nm and $L_z = 34.7$ nm.

Prior to the MD simulation, the block was uniformly expanded by the thermal expansion factor at the selected simulation temperatures. This expansion was intended to eliminate thermal stresses inside the grains. The equilibration MD runs were performed in the NPT ensemble (N, P and T denote the number of atoms, hydrostatic pressure and absolute temperature, respectively), with a Nosé–Hoover thermostat [26] and a Parrinello–Rahman barostat [27]. After the temperature reached the target value, the GB was equilibrated by an isothermal anneal for a few hundred picoseconds. The equilibration was followed by a production run in which the upper surface layer was moved parallel to the y-direction with a strain rate of $\sim10^8\,\text{s}^{-1}$. A 1 fs time integration step was used throughout this study. All the simulations performed in this study employed the LAMMPS (large scale atomic/molecular massively parallel simulator) code [28], and the atomic configurations visualized by ATOMEYE [29].

To investigate the GB mobility and the variation with the change in temperature, the GB velocity is extracted from the average positions of the front interface. The position of the GB is determined by utilizing the bond-angle distribution related order parameter (ADOP) developed by Ackland and Jones [30], i.e. the position of the grain boundary corresponds to a jump in the order parameter number when the ADOPs for each atom are plotted as a function of the y-position of the simulation box.

3. Results

3.1. Grain boundary motion under uniaxial loading with normal (90°) interface

3.1.1. Compression-driven GB migration

Previous studies [21] have linked the 90° lattice reorientation process to uniaxial compression (shockwave loading or nanoindentation). Here we focus on the evolution of the grain boundaries accompanying the lattice reorientation under uniaxial compression. An ideal 90° GB model with crystallographic orientations, $(10\bar{1}0)_{Grain2}$// $(0001)_{Grain2}$ // interface plane and $[1\bar{2}10]_{Grain1}$// $[1\bar{2}10]_{Grain2}$ is constructed as shown in Fig. 1b. The quasi-static compression stress is applied to the GBs by displacing the fixed atoms of the upper slab downwards with a constant velocity $v_n = 0.1$ A ps^{-1}. The compression-induced GB motion at 30 K is illustrated in Fig. 2. After the initial elastic deformation,
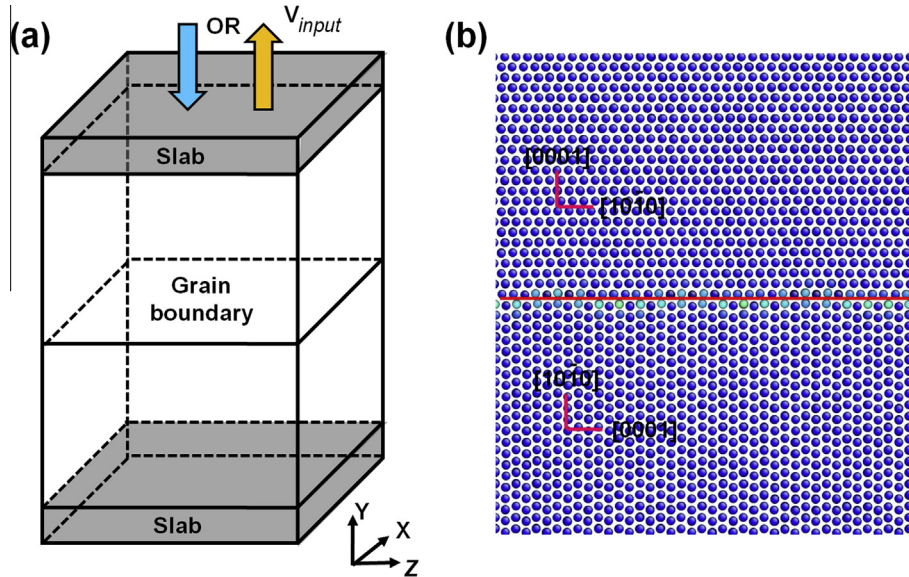
Fig. 1. Bicrystal simulation model used in the present work. (a) Geometry of the GB simulation block. The atoms in the gray slabs are fixed relative to each other and move as a rigid body. (b) Configurations of the grain boundary projected in the (y, z) plane, in which the bottom grain rotates 90° with respect to the upper grain.

a trapezoidal shaped interface is generated from the initial GB plane (Fig. 2b). This interface consists of an incoherent prismatic-basal boundary (IPB) and several coherent $\{10\bar{1}2\}$ twin boundaries (CTBs) as well as kinks. The IPB forms the front, where the atoms displace the most from the initial interface, and CTBs, which are symmetrically distributed on both sides. Under further loading, the migration of IPBs is accompanied by an increasing number of CTB segments. These CTB segments move cooperatively with the IPB, giving rise to the stable GB motion, as shown in Fig. 2c and d. The lattice regions left by the moving GBs were carefully examined for vacancies or any other lattice defects, and no extra defect generation was observed during the whole process.

In order to understand how the trapezoidal shaped interface is formed, we studied the nucleation mechanism by examining multiple snapshots stored during the MD simulations along with relevant parts of the atomic trajectories. A typical atomic configuration of the initial interface is shown in Fig. 3a. It involves two types of discrete interface dislocations, including the $\langle10\bar{1}1\rangle$ (blue and red color) and $\langle000\bar{1}\rangle$ (black color) modes. After the initial elastic deformation, a local atomic rearrangement (or lattice reorientation) occurs from the initial interface via a shear and shuffle mechanism akin to a martensitic transformation [31] (Fig. 3b), which leads to a disconnection with two atomic layers in height and six atomic layers in width. This rearrangement process is mediated by the gliding of one set of $[10\bar{1}1]$ interface dislocations through the receding grain. A second disconnection is generated by another set of $[\bar{1}011]$ slip modes (red) which become activated, and this glides across as the first disconnection is pinned and there is space available (Fig. 3c), thus forming an IPB with disconnections. Repetition of this process, which includes two different sets of dislocation arrays that do not interfere with each other, leads to the motion of the IPB. In addition, as the twin dislocations have the same orientation as the two sets of $\langle10\bar{1}1\rangle$ slips, they can also be activated from the interface and form a $\{10\bar{1}2\}$ CTB segment connecting

the IPB (Fig. 4d). Thus, a trapezoidal GB consisting of IPB and CTBs is formed via the composite action of two sets of $\langle10\bar{1}1\rangle$ dislocations and deformation twins.

3.1.2. Tensile-driven GB migration

For shear-driven coupled GB migration, it is known that by reversing the direction of the shear direction, each GB can move in the opposite direction with exactly the same normal boundary velocity [5]. Our previous study on the mechanism of the 90° GB motion mainly focused on the compression-driven case, where a large compressive strain can be obtained due to the lattice rearrangement from prismatic stacking to basal stacking. It is natural to consider whether this motion is reversible since a reverse lattice reorientation (basal stacking to prismatic stacking) can lead to a large tensile strain. Fig. 4 shows the tensile-driven 90° GB motion by reversing the loading direction. The GB moves into the upper grain with increasing tensile strain. A similar trapezoidal shape interface, which involves incoherent basal-prismatic boundary (IBP), IPBs and CTB segments, develops during the GB motion.

Fig. 5 compares the behavior of the time-dependent normal GB displacement of the IPB (GB front) at 30 K under three different external stress-driven conditions. The solid lines indicate the average GB velocities, v_n, as determined by the mean-square linear fits to the GB displacement data. Note that under uniaxial loading conditions (compression or tensile), the 90° GBs move either up or down with a constant average velocity v_n. This is a signature of the coupled motion and can be contrasted with the assumption that GBs in cubic metals do not move, but act either as pinning points or as dislocation sources under uniaxial loading [32–34]. In addition, the normal boundary velocities under compression ($v_n = 8.8$ A ps^{-1}) and tension ($v_n = -8.4$ A ps^{-1}) are not exactly the same, which indicates that the IPB and IBP have different mobilites. Interestingly, a zero normal GB displacement or pure rigid sliding is observed if shear is applied to the right of the upper slab with a constant velocity. This lack of motion with shear has been
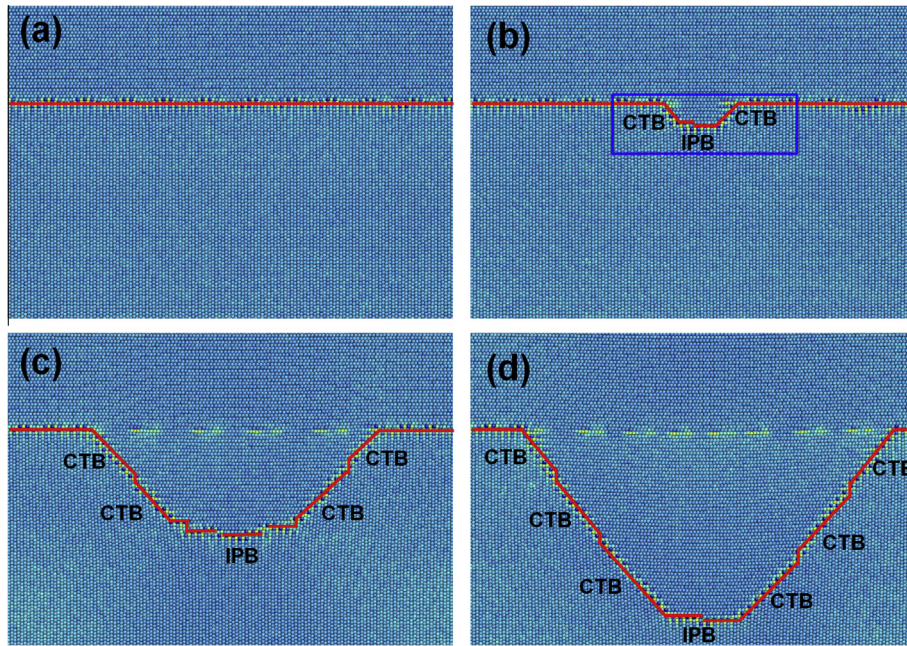
Fig. 2. The migration of the grain boundary separating crystal orientations differing by 90° under uniaxial compression at 30 K. (a) The initial bicrystal with planar interface. (b) The formation of a trapezoidal interface, which consists of incoherent prismatic-basal boundaries (IPBs) and coherent $\{10\bar{1}2\}$ twin boundaries (CTBs). (c, d) The grain boundary motion via the collective behavior involving IPB at the GB front and CTBs on the wings.
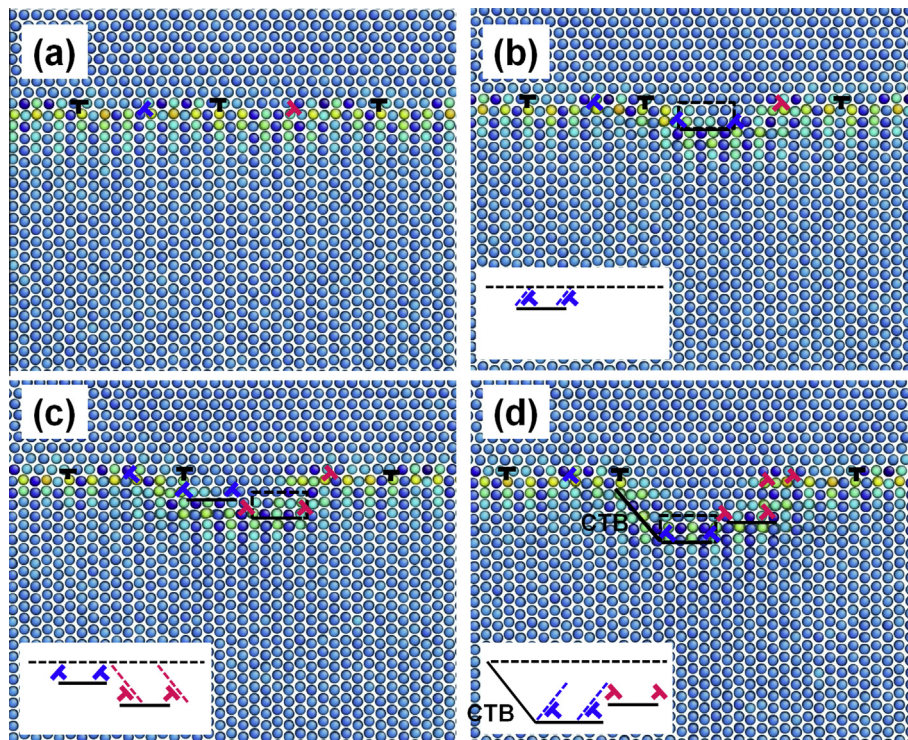
Fig. 3. The collective behavior of interface dislocations within the incoherent prismatic-basal boundary migration. (a) The bicrystal model with initial $\langle 10\bar{1}1 \rangle$ and $\langle 000\bar{1} \rangle$ dislocations; (b–d) two sets of $\langle 10\bar{1}1 \rangle$ dislocation arrays glide in a step-by-step manner. The dashed red and blue lines indicate the direction of slip for the two sets of dislocation arrays. (For interpretation of the references to colour in this figure legend, the reader is referred to the web version of this article.)
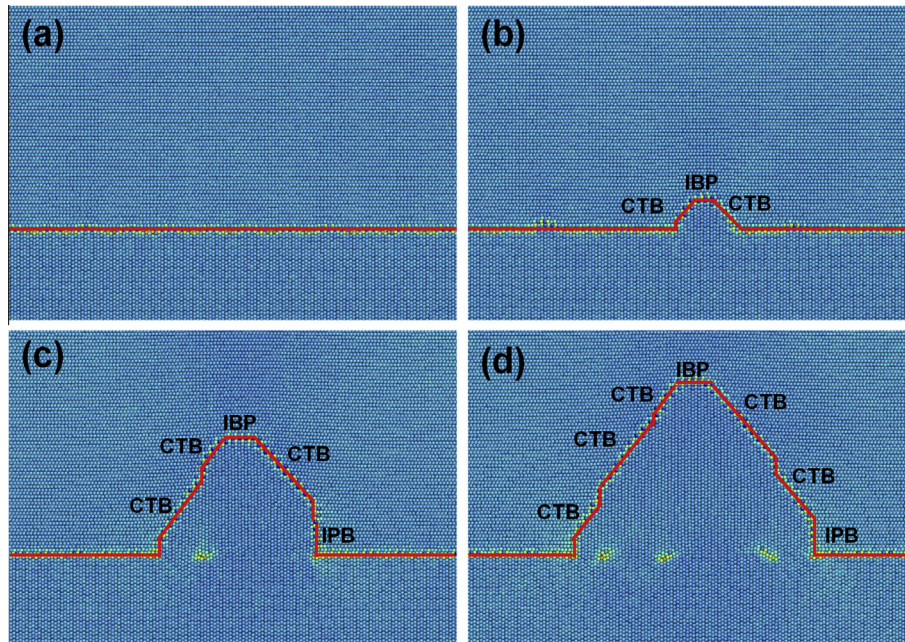
Fig. 4. Typical snapshots of MD simulations of tensile-induced motion of the 90° GB at 30 K. (a) The initial bicrystal with planar interface. (b) The formation of the trapezoidal interface, which also consists of an incoherent basal-prismatic boundary (IBP) at the front and coherent $\{10\bar{1}2\}$ twin boundaries (CTBs) on the wings, (c,d) The grain boundary motion via collective behavior involving IBP and CTBs.
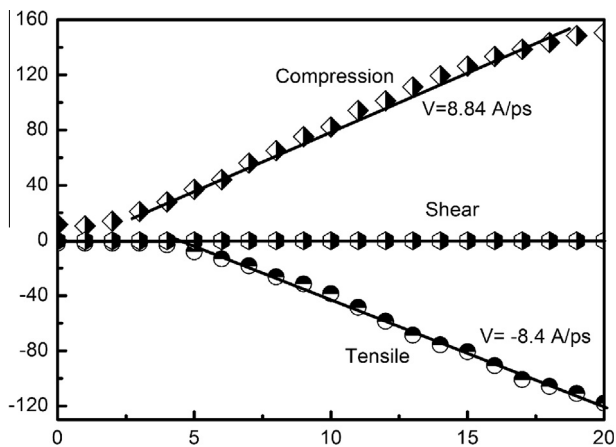
Fig. 5. GB displacement vs. time from MD simulations at 30 K under strain loading normal (uniaxial) or parallel (shear) to the GB plane. The strain rates of the compression and tensile loading are the same, $v_n = 0.1$ A ps^{-1}. Interestingly, the 90° GB cannot be driven by the shear stress.

also observed in fcc HAGBs at high temperatures due to the absence of collective glide of inclined dislocations [5]. However, two sets of inclined dislocation arrays are involved in the present study.

3.2. Grain boundary motion under uniaxial compression with tilted GBs

Grain boundary properties including grain boundary energy, diffusivity and mobility are sensitive to misorientation and inclination. Two tilted GBs are formed to examine the effects of uniaxial stress-driven coupling: one with 7° rotation while the misorientation between two grains is kept at 90° (Fig. 6a), and the other with a misorientation

of 97° (Fig. 6b). As shown in Fig. 8, the equilibrium GB plane is not flat and the tilted GB has a tendency to dissociate into many prismatic-basal segments to reduce the total GB energy. Under compression, trapezoidal interfaces can also be formed, indicating the occurrence of uniaxial coupled GB motion. However, debris and extra defects (such as dislocations and vacancies) are observed behind the moving GBs due to effects of the coupled GB motion and conventional plastic deformation process.

4. Discussion

4.1. Mechanism for GB motion under uniaxial stress

The stress-driven GB motion is expected to be similar to the migration of the phase boundary between the parent and product phase (habit plane) during the course of a martensitic transformation [31,35], where there is a cooperative action of habit plane motion and lattice transformation. The shape change (lattice-invariant plastic deformation) of the region in front of a habit plane is the result of the collective glide of dislocations or twins. Note that the interface remains approximately planar during a martensitic transformation as well as for shear-driven GB motion. In our case, the lattices of the parent and product "phases" are identical but only differ in their crystallographic orientation and GB motion is accompanied by a trapezoidal shaped interface. This interface can be dissociated into two parts: a planar front interface (including IPBs or IBPs) and two wings (containing CTBs and kinks), as shown in Fig. 7.

The migration of the trapezoidal interface can be understood as follows. We assume that interface dislocations play a major role in the uniaxial coupled GB motion. As illustrated schematically in Fig. 8, the migration of the front interface occurs by a two-step glide of discrete interface dislocations. These dislocations can be divided
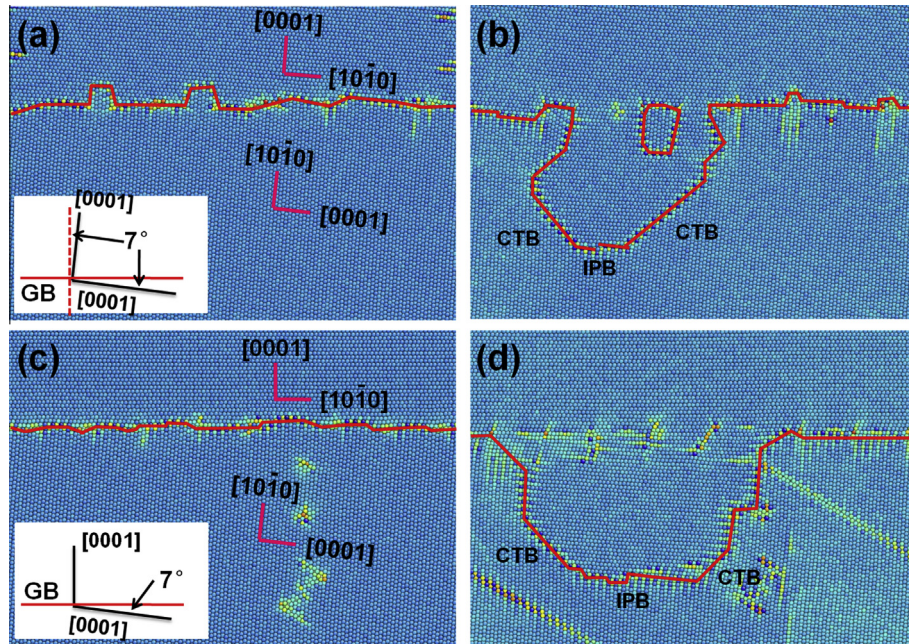
Fig. 6. Atomic configuration snapshot of tilted 90° grain boundary motion under uniaxial compression at 30 K. (a, b) The migration of an inclined 90° GB. (c, d) The migration of the misoriented 90° GB. A trapezoidal interface segment with IPB and CTBs is formed in both cases, indicating a similar uniaxial stress-driven coupling mechanism in tilted 90° GB.
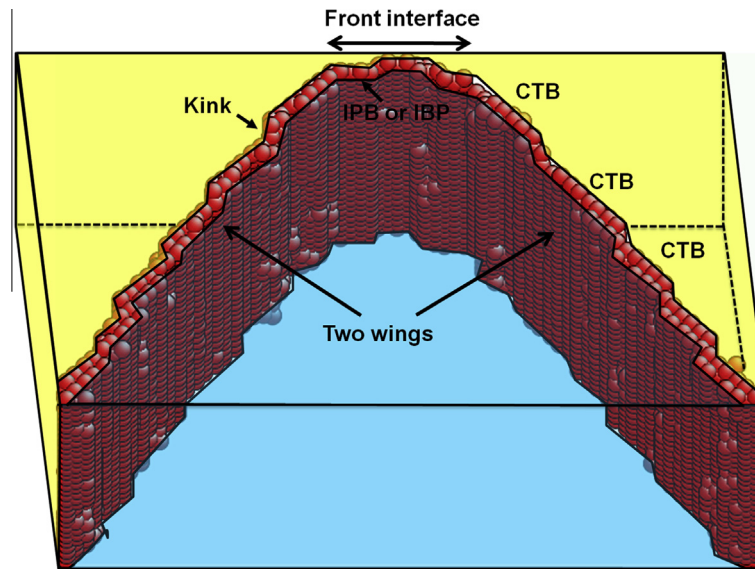
Fig. 7. Three-dimensional structure of the trapezoidal shaped GB. It consists of a front interface with incoherent prismatic-basal boundaries (IPBs) or incoherent basal–prismatic boundaries (IBPs), and two wings with coherent twin boundaries (CTBs) and dislocation kinks.
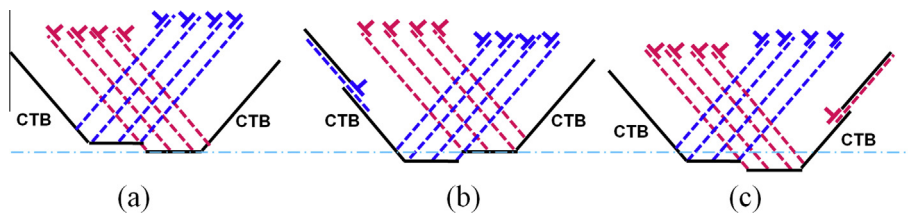
Fig. 8. Schematic illustration of the mechanism of uniaxial stress coupled GB motion. (a) Typical GB structure comprising CTBs and two sets of ⟨10$\bar{1}$1⟩ glide dislocation arrays. (b, c) Two sets of alternating glide dislocations as well as the interaction of dislocations with CTBs. The dashed red and blue lines indicate the direction of slip for the two sets of dislocation arrays. (For interpretation of the references to colour in this figure legend, the reader is referred to the web version of this article.)

into two sets (blue and red color). When the lattice reorientation events progress, two sets of dislocation arrays tend to glide step-by-step to avoid locking with each other, i.e., one set of dislocations moves forward while the other set remains in place (Fig. 8b, ensuring enough room for glide for the second set. When the slip planes of the remaining dislocations align with the glide room created, the dislocations glide forward recreating the initial GB structure (Fig. 8c).

This two-step slip process is similar to the asymmetric shear-driven coupled GB motion [36]. However, the uniaxial coupled motion is more complex as it involves a multiplication of deformation twins and an interaction of resultant CTBs with dislocations. The interaction can be explained as follows. When the dislocations glide on pyramidal planes incident on the CTBs, the <a + c> edge dislocation b will dissociate into a glissile twinning partial dislocation on the $\{10\bar{1}2\}$ twin plane with Burgers vector $b_t = s\{10\bar{1}1\}$ leaving a stair rod $b_r = b - b_t$ at the intersection of the glide and twin planes. The stair rod b_r can further dissociate into a twinning partial b_{t1} and another pyramidal dislocation b'. The above dislocation reactions at CTB generate a twinning dislocation or kink, and leave behind the original pyramidal dislocation at the twin boundary, as shown in Fig. 8b and c. This kink generation mechanism can thus promote the migration of the CTB segments.

The uniaxial stress-driven coupling can be further understood through the influence of inclined dislocations and twins. As shown in Fig. 8, the distribution of these dislocations and CTBs along the loading axis is symmetric. Take the deformation twins as an example. The GB is sheared forward in the plane normal to the loading axis by the passage of one group of CTBs (such as on the left wing in Fig. 7). The migration of the CTBs on the other wing will shear the GB in the opposite direction, giving rise to zero-net shear. In reality, the two groups of deformation twins occur simultaneously. The resulting deformation of the bicrystal represents a simple uniaxial compression or tensile normal to the GB plane.

4.2. Temperature-dependent coupling

So far we have only examined the coupled GB motion in response to the applied uniaxial stress at low temperatures.

We will now consider situations where the temperature increases. For shear-driven GB motion, the shear-driven coupling is characterized by the ratio of the tangential displacement to the normal displacement, referred to as the coupling coefficient. The shear-driven coupling coefficient is observed to decrease with increasing temperature as a result of the change of GB motion from coupling to sliding [5]. We define a uniaxial stress coupling parameter $\beta_u = v_n/v_a$, where v_n is the normal displacement of the interface front and v_a is the velocity of the fixed atoms of the upper boundary.

MD simulations of compression-driven GB motion were performed at temperatures up to 800 K below the hcp–body centered cubic (bcc) martensitic transformation temperature with the EAM potential of Ref. [25]. The position of the front interface (or IPB) is used to calculate the mobility of the 90° GB. Fig. 9a shows the plots of the time-dependent GB position with the same compression rate $v_a = 0.1$ A ps^{-1}. A linear relation of the GB position vs. time has been observed at all temperatures and the mobility of the boundary migration is extracted from the slope of these plots. The temperature dependence of the velocity is shown in Fig. 9b. The 90° GB mobility is found to decrease with increasing temperature in the range investigated, indicating a decreasing uniaxial stress-driven coupling at high temperatures.

GB motion is widely accepted to occur by a thermally activated process. In thermally activated GB motion, the mobility V follows an Arrhenius relationship with temperature for a given GB structure, such that $V = V_0 \exp(-Q/kT)$, where Q is the activation energy and V_0 is the constant prefactor related to an intrinsic frequency [37]. However, the velocity of the uniaxial stress-coupled GB is damped at high temperatures (Fig. 9b), implying a non-thermally activated motion process. In order to understand this non-thermal behavior, we analyzed the data for IPB position vs. time at selected temperatures. The inset of Fig. 10a shows the GB position as a function of time at 30 K. The 90° GB moves in a stop and go manner, indicating a very clear stick–slip behavior, which is well known in sliding friction. It is similar to shear-driven coupled GB motion where the boundary advances in a simple "stop–go" manner [38,39]. In our case, each period of the GB migration involves two "go" steps, i.e. "stop–go–go", which is consistent with the mechanism of two-step dislocation glide proposed here previously. Furthermore,
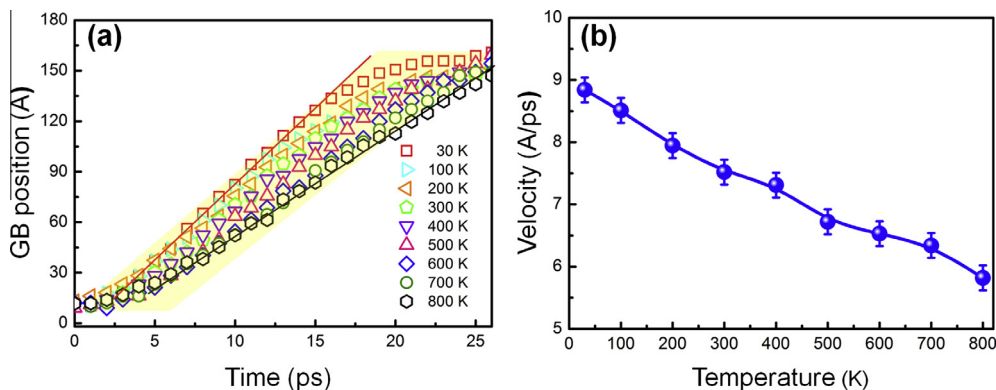
Fig. 9. Temperature-dependent GB mobility obtained from MD simulations with a loading rate of 0.1 A ps^{-1}. (a) Displacements of the front interface as functions of time at selected temperatures. (b) Temperature dependence of the normal velocity, v_n, of the 90° GBs, obtained by linear fitting from (a).
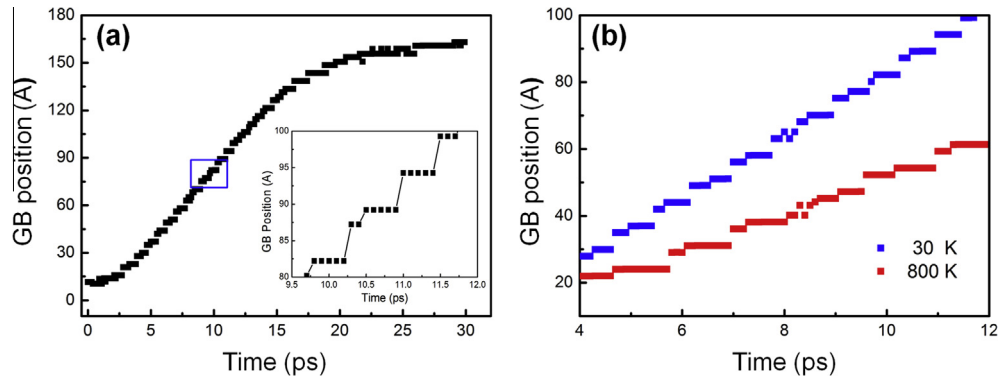
Fig. 10. The GB position as a function of time under uniaxial compression. The loading rate is 0.1 A ps^{-1}. (a) The time-dependent GB position at 30 K. The inset is an enlargement of the blue box region, illustrating the stick–slip character of the GB migration. (b) Comparison of the GB positions at low and high temperatures. A longer average pinning time is required for the high temperature case in a stop–go–go period. (For interpretation of the references to colour in this figure legend, the reader is referred to the web version of this article.)

the high temperature behavior is different. The time-dependent GB position for the shear-driven coupled motion becomes random as result of the increasing frequency of individual sliding events. However, a clear stick–slip character is observed for the uniaxial coupled case at high temperatures, as shown in Fig 10b, indicating that the coupled motion is not interrupted by occasional sliding events. Clearly, this represents a different, as-yet-uncharacterized coupling mechanism. We then compared the data for time-dependent GB position at 30 K and 800 K (Fig. 10b). The average pinning time at high temperature (red) is longer than that at low temperature (blue) during the uniaxial coupled motion, indicating that collective sliding events are suppressed as the temperature increases. However, a further understanding of the underlying mechanisms of such suppression is beyond the scope of the present study.

5. Conclusions

We investigated the migration of 90° grain boundaries in titanium bicrystals under an applied constant compression or tensile stress. Our atomistic simulations of uniaxial stress-driven GB motion show that the 90° GB moves via a composite action of dislocations and deformation twins. Interestingly, two types of dislocations belonging to different slip systems are formed during the GB migration, and the two sets of dislocation arrays tend to glide in a step-by-step manner. In addition, we find that the deformation behavior of titanium bicrystals is sensitive to GB inclination and GB misorientation.

A uniaxial stress-driven coupling is observed to govern the GB motion. This coupling is as a result of symmetrically distributed lattice defects (either dislocations or deformation twins), which counteract the shear component. Simulations of temperature dependent coupled motion show that the GB mobility or uniaxial stress-driven coupling decreases with increasing temperature. However, we find that the mechanism behind this temperature sensitivity is different from the shear-driven coupled GB motion where the GB motion changes from coupling to sliding as the temperature increases. We attribute this antithermal behavior to the decreasing frequency of collective sliding events. Although the observations presented and the associated conclusions are based on hcp-Ti, we believe that the uniaxial coupled mechanism applies to hcp metals in general.

References

[1] E.O. Hall, Proc. Phys. Soc. Lond. B 64 (1951) 747.
[2] N. Hansen, Scr. Mater. 51 (2004) 801.
[3] R. Armstrong, I. Codd, R.M. Douthwaite, N.J. Petch, Philos. Mag. 7 (1962) 45.
[4] A.-K. Maier, D. Mari, I. Tkalcec, R. Schaller, Acta Mater. 74 (2014) 132.
[5] J.W. Cahn, J.E. Taylor, Acta Mater. 52 (2004) 4887.
[6] J. Li, A.K. Soh, Acta Mater. 61 (2013) 5449.
[7] L. Wang, J. Teng, P. Liu, A. Hirata, E. Ma, Z. Zhang, et al., Nat. Commun. 5 (2014).
[8] V. Yamakov, D. Wolf, S.R. Phillpot, A.K. Mukherjee, H. Gleiter, Nat. Mater. 3 (2004) 43.
[9] J. Schiotz, F.D. Di Tolla, K.W. Jacobsen, Nature 391 (1998) 561.
[10] T.J. Rupert, D.S. Gianola, Y. Gan, K.J. Hemker, Science 326 (2009) 1686.
[11] Y. Zhang, J.A. Sharon, G.L. Hu, K.T. Ramesh, K.J. Hemker, Scr. Mater. 68 (2013) 424.
[12] A. Rajabzadeh, M. Legros, N. Combe, F. Mompiou, D.A. Molodov, Philos. Mag. 93 (2013) 1299.
[13] V.A. Ivanov, Y. Mishin, Phys. Rev. B. 78 (2008).
[14] A. Rajabzadeh, F. Mompiou, M. Legros, Combe N, Phys. Rev. Lett. 110 (2013).
[15] M.J. Rahman, H.S. Zurob, J.J. Hoyt, Acta Mater. 74 (2014) 39.
[16] H.A. Khater, A. Serra, R.C. Pond, J.P. Hirth, Acta Mater. 60 (2012) 2007.
[17] J.W. Cahn, Y. Mishin, A. Suzuki, Acta Mater. 54 (2006) 4953.
[18] S.E. Babcock, R.W. Balluffi, Acta Metall. 37 (1989) 2367.
[19] J. Wang, Q. Yu, Y. Jiang, I.J. Beyerlein, Jom 66 (2014) 95.
[20] H. Zhang, J. Mater. Res. 24 (2009) 3446.
[21] H. Zong, X. Ding, T. Lookman, J. Li, J. Sun, E.K. Cerreta, et al., Phys. Rev. B. 89 (2014).
[22] W.Z. Han, Q. An, S.N. Luo, T.C. Germann, D.L. Tonks, W.A. Goddard III, Phys. Rev. B. 85 (2012).
[23] S.-N. Luo, T.C. Germann, D.L. Tonks, Q. An, J. Appl. Phys. 108 (2010).

[24] B.-Y. Liu, J. Wang, B. Li, L. Lu, X.-Y. Zhang, Z.-W. Shan, et al., Nat. Commun. 5 (2014).

[25] R.R. Zope, Y. Mishin, Phys. Rev. B. 68 (2003).

[26] G.J. Martyna, M.L. Klein, M. Tuckerman, J. Chem. Phys. 97 (1992) 2635.

[27] M. Parrinello, A. Rahman, Phys. Rev. Lett. 45 (1980) 1196.

[28] S. Plimpton, J. Comput. Phys. 117 (1995) 1.

[29] J. Li, Model. Simul. Mater. Sci. Eng. 11 (2003) 173.

[30] G.J. Ackland, A.P. Jones, Phys. Rev. B. 73 (2006).

[31] C.M. Wayman, MMTA 25 (1994) 1787.

[32] P.J. Imrich, C. Kirchlechner, C. Motz, G. Dehm, Acta Mater. 73 (2014) 240.

[33] S.J. Fensin, J.P. Escobedo-Diaz, C. Brandl, E.K. Cerreta, G.T. Gray Iii, T.C. Germann, S.M. Valone, Acta Mater. 64 (2014) 113.

[34] N. Kheradmand, H. Vehoff, A. Barnoush, Acta Mater. 61 (2013) 7454.

[35] K. Otsuka, X. Ren, Prog. Mater. Sci. 50 (2005) 511.

[36] Z.T. Trautt, A. Adland, A. Karma, Y. Mishin, Acta Mater. 60 (2012) 6528.

[37] E.R. Homer, E.A. Holm, S.M. Foiles, D.L. Olmsted, Jom 66 (2014) 114.

[38] Y. Mishin, A. Suzuki, B.P. Uberuaga, A.F. Voter, Phys. Rev. B. 75 (2007).

[39] Q. Hu, L. Li, N.M. Ghoniem, Acta Mater. 57 (2009) 4866.